https://doi.org/10.1016/j.tws.2021.108211

Compressive behaviour and design of compact to slender octagonal concrete-filled steel tubular stub columns

Junbo Chen[1,2], Tak-Ming Chan[3,4]*

[1]School of Civil and Hydraulic Engineering, Huazhong University of Science and Technology, Wuhan, Hubei province, China
[2]Formerly, Department of Civil and Environmental Engineering, The Hong Kong Polytechnic University, Hung Hom, Hong Kong, China
[3]Department of Civil and Environmental Engineering, The Hong Kong Polytechnic University, Hung Hom, Hong Kong, China
[4]Chinese National Engineering Research Centre for Steel Construction (Hong Kong Branch), The Hong Kong Polytechnic University, Hung Hom, Hong Kong, China
*Corresponding author: tak-ming.chan@polyu.edu.hk

Abstract: This paper presents an experimental investigation into the compressive behaviour of compact to slender octagonal concrete-filled steel tubular (OctCFST) stub columns. In this study, a total of twenty OctCFST stub column specimens were tested. Five octagonal hollow sections with various cross-sectional slenderness were fabricated from 3 mm and 6 mm 460 steel plates. The measured yield strengths of the two batches of steel plates are 546.5 and 580.7 MPa, respectively. Three grades of concrete with measured cylinder strengths varying from 27.9 to 92.1 MPa were used to infill the hollow tubes. The test results, in terms of failure modes, axial load versus axial strain responses and cross-sectional capacities of the stub column tests are fully presented and discussed. The experimental results were then used to evaluate the applicability of current design methods in Eurocode EN 1994-1-1, American standard ANSI/AISC 360-16, Chinese code GB 50936-2014 and equivalent circle methods. It is shown that the circumcircle method and GB 50936-2014 approach produce excellent cross-sectional strength predictions for the OctCFSTs and the current cross-section slenderness limit of $135\times235/f_y$ for circular concrete-filled steel tubes specified in GB 50936-2014 can be safely extended to the design of OctCFSTs when the equivalent circumcircle method is used.

Keywords: Stub column; Octagonal section; CFST; Design; slenderness limit.

1. Introduction

In recent years, polygonal steel hollow sections, such as octagonal hollow sections (OctHSs), have attracted significant interests from researchers and structural engineers [1]. An obvious attraction of OctHSs is the reduced flat side width when compared to square or rectangular hollow section (SHS/RHS) counterparts with same perimeter [2, 3]. OctHSs therefore exhibit stronger local buckling resistances. The flat surfaces in OctHSs also provide easier beam-to-column connection constructions when compared to circular hollow sections (CHSs) [2, 3]. In addition, the bend angle of regular OctHSs at each corner is 45°, only half of SHS/RHS counterparts, making OctHSs easier to be cold-bent, and the plastic deformation at corner portions of OctHSs is smaller. This advantage improves its potential in cold-formed sections, particularly when high strength steels are employed.

OctHS columns have been adopted in many civil engineering applications such as transmission poles, telegraph towers and lattice structures [4, 5]. An example of the use of OctHSs is depicted in Fig. 1. Design provisions for OctHSs have been specified in an ASCE standard for steel transmission pole structures (ASCE/SEI 48-11 [6]). However, design of OctHSs is not included in any current structural steel design specifications like Eurocode EN 1993-1-1 [7] and American standard ANSI/AISC 360-16 [8]. To date, extensive experimental investigations have been carried out to study the behaviour of OctHSs at material property level [4, 9] and cross-section level [2, 3, 10-12]. Chen et al. [1] collected a test database on OctHS stub columns and conducted a comprehensive parametric study. Detailed design rules for cross-sectional strengths of OctHSs under compression have been subsequently proposed in [1].

The applications of OctHSs in composite structures, such as concrete-filled steel tubular (CFST) members, have also attracted the attention of researchers [13-19]. In CFSTs, the circular shaped

steel tubes provide a uniform confining pressure to concrete core, efficiently confining the infilled concrete and improving both the strength and ductility of concrete, while rectangular shaped tubes provide flat surfaces to allow various types of beam-column connections, like bolted connection with end plates. Octagonal concrete-filled steel tubular (OctCFST) columns can combine the merits of both circular and rectangular CFSTs, providing comparable confinement as circular CFSTs while maintaining the constructability [15]. The first research on OctCFST stub columns can date back to 1977 [20], in which a total of 268 CFST stub columns were tested, including 148 circular CFSTs, 60 square CFSTs and 60 OctCFSTs. In this study, the OctCFST specimens were made of normal strength materials with steel yield strength f_y varying from 294 to 341 MPa and with concrete cylinder strength f_c' ranging from 16.7 to 30.1 MPa. Since then, more experimental investigations [14-18] into OctCFST members have been carried out. Ding et al. [14] carried out eight OctCFST stub column tests and the specimens were prepared using normal strength steel and normal strength concrete with f_y of about 311-321 MPa and concrete cube strength f_{cu} of 39.3 and 57.4 MPa. Zhu and Chan [15, 16] tested nine OctCFST stub columns made of normal strength steel with f_y of 296-383 MPa. Both normal strength and high strength concretes with f_c' varying from 37.7 to 113.5 MPa were investigated. Lim and Eom [19] conducted eight thin-walled irregular OctCFST stub column tests with different tube wall slenderness ratios. The stub columns were made of normal strength steel with f_y of 407-489 MPa and normal strength concrete with f_c' of 33.0 MPa. It is noted that these existing experimental investigations have focussed on mild steels. Research on OctCFST stub columns using higher strength steels (with f_y higher than 460 MPa), in particular for thin-walled regular sections, remains extremely scarce, potentially inhibiting attempts to develop effective design recommendations. At present, design of OctCFST members is only specified in Chinese code GB 50936-2014 [21], but the cross-section slenderness

limits are not specified. Design of OctCFST members is not covered in any other design codes such as Eurocode EN 1994-1-1 [22] and American standard ANSI/AISC 360-16 [8]. It is unclear neither whether the current cross-section slenderness limits for circular, square and rectangular CFSTs are applicable to OctCFSTs. It is therefore of great interest to provide experimental evidence and develop effective design rules to promote the application of OctCFSTs.

The primary objective of this paper is to further experimentally investigate the compressive behaviour of compact to slender OctCFST short columns made of steels with f_y higher than 460 MPa. A total of twenty specimens with different cross-sectional slenderness were prepared and tested. Two batches of 460 steel with nominal thickness of 3 mm and 6 mm were employed to fabricate the octagonal tubes. Three concrete grades, namely, C30, C50 and C90, were used to infill the tubes. The experimental results in terms of failure modes, cross-sectional capacities and ductility are discussed. The test results were employed to evaluate the applicability of EN 1994-1-1 [22], ANSI/AISC 360-16 [8], and GB 50936-2014 [21] and equivalent circle methods [15] to the design of OctCFSTs studied herein.

2. Experimental investigations

2.1 Specimens

In this test programme, twenty octagonal concrete-filled steel tubular (OctCFST) stub columns were prepared and tested. Five octagonal steel hollow sections (OctHSs) with different cross-sectional slenderness were considered. The OctHSs were fabricated by welding two cold-formed half-sections on flat surfaces. The cold-formed half-sections were press-braked using 3 mm and 6 mm thin 460 steel plates. Detailed fabrication procedures have been described elsewhere in Chen et al. [3] (see CF2). Three concrete grades, namely, C30, C50 and C90 with target compressive

97 cylinder strengths of 30, 50 and 90 MPa, respectively, were used to infill the octagonal tubes.
98 Definitions of symbols for OctCFSTs are demonstrated in Fig. 2, where D is the outer diameter
99 (termed as the circumcircle diameter for equivalent circle method detailed in later section), H is
100 the overall width (also termed as the inscribed circle diameter), B is the side width, b is the clear
101 width excluding corner portions, t is the thickness of the tube, and r_o and r_i are the outer and inner
102 corner radii, respectively.

103 For a regular OctHS, the relations among the side width B, the overall width H and the maximum
104 outer dimension D are formulated in Eqs. (1) and (2).

$$B=\left(\sqrt{2}-1\right)H \tag{1}$$

$$D=\sqrt{H^2+B^2} \tag{2}$$

105 The clear width b can be obtained by Eq. (3), where θ is the interior angle of OctHS, which is
106 equal to $\pi/8$, as shown in Fig. 2(b),

$$b = B\text{-}2r_o \cdot \tan\theta \tag{3}$$

107 The cross-sectional areas of steel A_s and concrete A_c of OctCFSTs were calculated from Eqs. (4)
108 and (5).

$$A_s = 8\times b\times t+\pi\left(r_o^2-r_i^2\right) \tag{4}$$

$$A_c = 8\times\frac{1}{2}\times\frac{H-2t}{1+\sqrt{2}}\times\frac{H-2t}{2}-8\times\frac{1}{2}\times\frac{2r_i}{1+\sqrt{2}}r_i+\pi r_i^2 \tag{5}$$

109 Table 1 summarises geometric properties of the OctCFST specimens. The length L of the
110 specimens is designed equal to $3H$ to ensure that all the specimens are stub columns [23]. Table 1
111 also presents the steel ratio ρ of each specimen, which is defined as the ratio of steel area A_s over
112 total cross-sectional area A_s+A_c. As shown, the steel ratio ρ varies from 4.6% to 12.0%, most of

which is relatively low (4.6% ~ 8.1%) when compared to those of conventional CFST columns [19]. It should be noted that a wide range of $b/(t\varepsilon)$ ratios from 18.3 to 50.7 is covered in the test programme, in which ε is the material coefficient depending on f_y ($\varepsilon = \sqrt{235/f_y}$). To further evaluate the compactness of the OctCFST specimens, two ratios are presented in Table 1 as well, namely, overall width-to-thickness ratio H/t and circumcircle diameter-to-thickness ratio D/t. Cross-section classification of these sections according to different criteria is presented in Table 1. A specimen label system is used throughout this study, which firstly specifies the cross-sectional shapes of the specimen, "O" for OctCFSTs. Following the cross-sectional shape, cross-sectional dimensions are given by "B×t". The digit after the hyphen represents the grade of infilled concrete. For example, the label "O75×6-90" designates an OctCFST specimen having a nominal side width and thickness of 75 and 6 mm, respectively, and infilled with C90 concrete. The symbol "#" in the suffix indicates a repeated test, which is designed to verify the accuracy and repeatability of the experimental tests.

2.2 Material properties

2.2.1 Steel

To obtain material properties of steel, three tensile coupons were extracted from the parent plates of each batch of steel plates. The tensile coupon tests were carried out in accordance with EN ISO 6892-1:2019 [24]. Strain gauges were affixed to determine the elastic modulus and the Poisson's ratio. An extensometer was attached to record full stress-strain responses up to fracture. During each tensile coupon test, the loading was paused twice near yield strength and ultimate strength for 120 seconds to allow for stress relaxation to obtain the static stress-strain curves. The obtained static stress-strain curves were then used to determine the static material properties, such as yield

strength and ultimate strength. Detailed descriptions of the coupon tests can be found elsewhere in Chen et al. [4]. Mean measured material properties are tabulated in Table 2, in which E_s is the elastic modulus, v is the Poisson's ratio, f_y is the yield strength, f_u is the ultimate strength, ε_u is the strain at the ultimate strength, ε_{sh} is the strain-hardening strain at which strain-hardening initiates and ε_f is the proportional elongation at fracture. The yield strengths of the 3 mm and 6 mm steel plates are 546.5 MPa and 580.7 MPa, respectively. Typical full stress-strain curves of parent metals are shown in Fig. 3.

2.2.2 Concrete

Material properties of concrete were obtained from standard cylinders with a diameter of 150 mm and a height of 300 mm. The concrete cylinders were prepared during the concrete infilling of specimens. The cylinders were tightly wrapped with cling film after demoulding and the wrapped cylinders were stored besides the OctCFST specimens to simulate the curing conditions of the infilled concrete core [17, 18]. For each batch of concrete, three cylinders were prepared and tested at the test day of corresponding OctCFST specimens to obtain the exact compressive strengths. Four strain gauges with a gauge length of 90 mm were attached onto the surface of each cylinder. Two strain gauges were mounted longitudinally to obtain stress-strain curves and the elastic modulus, while the other two were put in the hoop direction to determine the Poisson's ratio of concrete. The cylinders were tested under displacement control at a rate of 0.15 mm/min, which is equivalent to the initial strain rate (0.05% min^{-1}) of tensile coupon tests, and the testing procedure complied with EN 12390-3 [25]. Table 3 summarises the test results, i.e. elastic modulus E_c, Poisson's ratio v_c, compressive cylinder strength f_c', axial strain at compressive strength ε_c, and coefficient of variation (CoV) of the concrete elastic modulus and compressive strength. It should be noted that the C30 specimens were prepared in two batches. Therefore, two compressive

cylinder strengths for C30 concrete are reported in Table 3, marked as C30-1 and C30-2, respectively. Typical stress-strain curves of the used concrete are presented in Fig. 4.

2.3 Stub column tests

The stub column tests were carried out to investigate the compressive behaviour of OctCFSTs. The investigating parameters are the cross-section slenderness and the strength of infilled concrete. The stub column specimens were prepared and tested at The Hong Kong Polytechnic University. All OctHSs had both ends milled flat and perpendicular to the longitudinal axis before concrete casting and high strength gypsum was used to fill the gap at the top surface between the steel tube and concrete infill to obtain flat end surfaces; hence, a uniform compressive load can be ensured during the test. The stub column specimens were compressed at a constant displacement rate of 0.05%L mm/min, which is equivalent to the initial strain rate (0.05% min^{-1}) for tensile coupon tests and the strain rate for concrete cylinder tests. Strain gauges were mounted at the mid-height of each specimen and four linear variable displacement transducers (LVDTs) were located between two parallel end-plates to record the end shortening of the stub columns. The arrangements of strain gauges and LVDTs as well as the test set-up are depicted in Fig. 5. End shortening was obtained by combining the strain gauge data with the LVDT readings. Strain gauge readings were used to modify the initial stage of LVDT readings, thereby giving true specimen end shortening. The axial strain of each test can be then obtained by dividing the modified LVDT readings by the length of column L.

3 Test results

3.1 Failure modes

All the tested OctCFST stub columns failed by outward local buckling of the steel tubes and shear failure of concrete cores. Typical failure modes of the outer steel tube and concrete core (specimen O75×3-90) are presented in Fig. 6.

3.2 Axial load versus axial strain curves and cross-sectional strengths

The axial load versus axial strain curves of all the OctCFST stub column tests are shown in Fig. 7. The corresponding octagonal hollow section (OctHS) test results, which have been reported in a companion paper [3], are plotted in Fig. 7 as well for comparison. Five repeated tests (specimens ended with #) were conducted. The repeated specimens exhibit consistent axial load versus axial strain curves with a maximum difference on the ultimate load of 3.5%, thereby confirming the reliability and repeatability of the test programme. Key testing parameters and experimental results of each specimen are summarised in Table 4, including the yield strength of steel f_y, compressive cylinder strength of concrete f_c', confinement ratio θ, nominal squash load N_0 (equal to $A_s f_y + A_c f_c'$), ultimate load N_u and ultimate axial strain ε_u (strain corresponding to N_u). The confinement ratio θ is an important indicator to evaluate the level of confinement in CFST members [26], and it is defined as the ratio of steel contribution over concrete contribution, as given by $A_s f_y / A_c f_c'$. As can be observed from Fig. 7 and Table 4, with the same cross-section size, higher ultimate loads N_u of 66–431% were obtained for the OctCFST specimens when compared to hollow counterparts. Besides, with the increase of f_c' for each cross-section, the load dropped more rapidly after N_u was attained due to the brittleness of high strength concrete and reduced confinement effect.

To assess the confinement effect in the OctCFST specimens, a strength index (*SI*), which has been used by Han [27], was adopted, as expressed in Eq. (6),

$$SI = \frac{N_u}{N_0} \tag{6}$$

where N_0 is the nominal squash load and can be calculated by a summation of the steel and concrete contributions as $A_s f_y + A_c f_c'$. The *SI* of each specimen is listed in Table 4. The *SI* value of all specimens is greater than unity with a maximum value of 1.29 and a minimum value of 1.02. The mean value of *SI* is 1.21 and the corresponding coefficient of variance (CoV) is 0.06, indicating that the strengths of both steel and concrete are fully utilised. The *SI* is plotted with respect to confinement ratio θ in Fig. 8(a). As demonstrated, the *SI* generally increases with the increase of confinement ratio θ owing to the improved confinement effect. Fig. 8(b) depicts the influence of confinement ratio θ on the ultimate axial strain ε_u. It can be observed that the better the confinement is, the larger ultimate axial strain ε_u is obtained.

To evaluate the effect of cross-section slenderness on the performance of the OctCFSTs, the strength index *SI* and the ultimate axial strain ε_u are plotted against the cross-section slenderness. The circumcircle diameter-to-thickness ratio D/t is used herein for illustration. As displayed in Fig. 9(a) and 9(b), *SI* and ε_u in each concrete series decrease with the increase of the D/t ratio, primarily due to the reduced confinement effectiveness.

Referring to Figs. 8 and 9, the ultimate axial loads N_u of some OctCFST specimens with higher confinement ratio θ were attained at quite large axial strains. For example, the ultimate axial strain ε_u of specimen O75×6-30 can be as high as 4.5% (θ = 2.85). Current design codes, such as ANSI/AISC 360-16 [8], EN 1993-1-1 [7] and Chinese code GB 50936-2014 [21] clearly target at the control of yielding of cross-sections in design to avoid development of excessive deformation in structural members. In this study, a deformation limit criterion of 1.0% axial strain for ultimate

limit state is adopted, in accordance with the recommendation in [28, 29]. Similar design concept of deformation limit has been adopted in the design of tubular joints [30] and design of fibre reinforced polymer (FRP) confined concrete columns [31]. The failure load N_f was determined from the first occurrence of N_u or $N_{1.0\%}$ (the applied load at 1.0% axial strain), as illustrated in Fig. 10. The obtained $N_{1.0\%}$ and N_f are reported in Table 4.

3.3 Ductility

The ductility of the OctCFST specimens was appraised by a ductility index (*DI*) defined in Eq. (7), following the approach used by [27, 32],

$$DI = \frac{\varepsilon_{85\%}}{\varepsilon_u} \tag{7}$$

in which $\varepsilon_{85\%}$ is the axial strain when the applied axial load drops back to 85% of the ultimate load N_u and ε_u is the ultimate axial strain at ultimate load. The obtained ductility index (*DI*) of each specimen is listed in Table 4. As per the definition, a lower *DI* value means that the load falls rapidly in the post-peak range, whilst a higher value indicates a stronger ability to maintain at least 85% of the ultimate load N_u. As shown in Fig. 7, the axial load of some specimens with higher confinement ratios exhibits a slow degradation in the post-peak range and even does not decrease below 85% of N_u. For these specimens, the *DI* cannot be obtained. In this study, an equivalent yield strain for the OctCFSTs $\varepsilon_{y,sc}$ was proposed, which is similar to the definition of steel yield strain ε_y (=f_y/E_s), and can be calculated from Eq. (8).

$$\varepsilon_{y,sc} = \frac{N_0}{(EA)_{sc}} \tag{8}$$

where $(EA)_{sc}$ is the compressive stiffness of composite sections, determined from a linear regression of load over strain between 10% and 40% of N_0, same as the determination of modulus

of elasticity of metallic materials [24]. The theoretical value of compressive stiffness can be determined from $E_sA_s+E_cA_c$, denoted as $(EA)_{sc,Cal}$. The compressive stiffness obtained from test results and theoretical calculation is given in Table 4. The compressive stiffness determined from regression is close to calculated values, having a mean $(EA)_{sc}/(EA)_{sc,cal}$ value of 0.98. Table 4 tabulates the obtained yield strain $\varepsilon_{y,sc}$ and $\varepsilon_u/\varepsilon_{y,sc}$ of each specimen. The $\varepsilon_u/\varepsilon_{y,sc}$ values are plotted with regard to the confinement ratio θ in Fig. 11. As shown, the $\varepsilon_u/\varepsilon_{y,sc}$ values generally increase with confinement ratio θ because of the improved confinement.

3.4 Comparison of compressive behaviour between circular CFST and OctCFST columns

The compressive behaviours of six circular CFST stub columns available in the literature [33] were selected to compare with OctCFST specimens having similar parameters tested in the current study. The tubes in [33] were obtained using the same batches of steel plates as those used for fabricating the octagonal tubes in this study. However, the measured steel yield strengths in [33] are higher than those in this study because of the cold forming effect during fabrication process. It is worth noting that the selected circular and octagonal specimens are not exact equivalent due to the differences in material and geometric properties. Hence, particular attention has been paid to select the most suitable test specimens in order to obtain qualitative observations. The 4C200×3 and 4C200×6 series in [33] are comparable to the O75×3 and O75×6 series in this study. The test parameters of the selected test specimens, including geometric parameters such as the diameter, thickness and length of steel tubes, D, t and L, material parameters like f_y and f_c' and test results such as N_u and ε_u are summarised in Table 5.

The axial load N of the six pairs of circular and octagonal CFSTs is normalised by the nominal squash load N_0 and plotted against the axial strain in Fig. 12. As can be observed from Table 5 and

Fig. 12, the confinement in octagonal CFSTs in terms of *SI* is less effective than that in circular CFSTs under higher confinement ratios (C30 and C50 pairs). When high strength concrete was used (C90 pairs), the confinement effectiveness in octagonal CFSTs is comparable to circular counterparts and the difference in *SI* becomes negligible. With regard to the ductility, the load of circular CFSTs (except for $D/t \approx 34$, $f_c' \approx 30$ MPa pair) drops more slowly than OctCFSTs, indicating that circular CFSTs have better post-peak behaviour than OctCFSTs.

4. Current design methods and assessment

4.1 Existing codes of practice

Design codes around the world, such as Eurocode EN 1994-1-1 [22], American standard ANSI/AISC 360-16 [8] and Chinese code GB 50936-2014 [21], provide design equations for calculating the cross-sectional resistance of CFST members. However, the design of OctCFST members is not covered in neither Eurocode EN 1994-1-1 nor American standard ANSI/AISC 360-16. Though Chinese code GB 50936-2014 gives design formula for OctCFST members, cross-section slenderness limit is not specified. It is still unclear if current limits for circular and square CFSTs are valid for OctCFSTs. It has been found by Chen et al. [1] that the current cross-sectional slenderness limits for square and rectangular hollow sections are not applicable to the design of OctHSs. This is largely because the angle of adjacent tube walls in octagonal sections is 135° and the edges of the tube wall are considered as partially clamped when compared to those with 90° angle [19]. It may be expected the current cross-sectional slenderness limits for square or rectangular CFSTs are not suitable for OctCFSTs neither. To classify the octagonal sections, as discussed in [15, 19], two equivalent circle methods might be adopted, namely, circumcircle method (D/t) and inscribed circle method (H/t). It is noted that the circumcircle method gives a

slightly large equivalent diameter-to-thickness ratio (D/t) than the inscribed circle method (H/t), which tends to be conservative in design. Thus, the circumcircle method is used in this study. As for the design of circular CFSTs, EN 1994-1-1 and GB 50936-2014 specify the maximum diameter-to-thickness D/t values, i.e. $90\times235/f_y$ and $135\times235/f_y$ to avoid local buckling of steel tubes. ANSI/AISC 360-16 classifies circular CFSTs into compact, noncompact and slender sections with corresponding limiting D/t values of $\lambda_p = 0.15E_s/f_y$, $\lambda_r = 0.19\,E_s/f_y$ and $\lambda_{max} = 0.31E_s/f_y$. λ_p, λ_r and λ_{max} are the compact-to-noncompact, noncompact-to-slender and maximum permitted D/t ratios, respectively. Assuming E_s = 200 GPa, the equivalent limiting D/t values are $\lambda_p = 128\times235/f_y$, $\lambda_r = 162\times235/f_y$ and $\lambda_{max} = 264\times235/f_y$, respectively. The cross-section classification of each specimen according to the equivalent circumcircle method is presented in Table 4. As shown, the experimental tests include a wide range of cross-sectional slenderness, covering compact to slender sections. The cross-section slenderness limit and other requirements set by the design codes, such as material strength limitations on both concrete and steel, are summarised in Table 6, in which δ is the steel contribution ratio (defined in Eq. (9)) and ρ is the steel ratio. These design equations are discussed and evaluated in this section.

$$\delta = \frac{A_s f_y}{A_s f_y + A_c f_c'} \tag{9}$$

4.1.1 EN 1994-1-1 [22]

In EN 1994-1-1, two design methods are standardised. The first method (Method 1) simply superposes the strengths of concrete and steel to determine the cross-sectional strength of CFST columns ($N_{EC4,1}$), as formulated in Eq. (10), while the second method (Method 2) fully takes account of the benefits of confinement in circular CFSTs. The cross-sectional strength ($N_{EC4,2}$) is calculated from Eq. (11), in which η_a is a reduction factor applied to the axial strength of steel tube due to the biaxial state of steel, and η_c is a magnified factor multiplied to concrete to consider the

strength enhancement in concrete due to confinement. These factors are affected by the relative slenderness $\bar{\lambda}$ and eccentricity of the column as per EN 1994-1-1. In case of uniaxial compression, the factors η_a and η_c can be calculated from Eqs. (12) and (13), respectively. The relative slenderness $\bar{\lambda}$ can be determined according to EN 1994-1-1.

$$N_{EC4,1} = A_s f_y + A_c f_c^{'} \tag{10}$$

$$N_{EC4,2} = \eta_a A_s f_y + \left(1 + \eta_c \frac{t f_y}{D f_c^{'}}\right) A_c f_c^{'} \tag{11}$$

$$\eta_a = 0.25\left(3 + 2\bar{\lambda}\right) \leq 1 \tag{12}$$

$$\eta_c = 4.9 - 18.5\bar{\lambda} + 17\bar{\lambda}^2 \geq 0 \tag{13}$$

4.1.2 ANSI/AISC 360-16 [8]

A series of design equations (Eqs. (14) to (16)) are provided in ANSI/AISC 360-16 to estimate the cross-sectional strength of CFST columns (N_{AISC}), depending on the cross-section classification of the steel tube. For compact sections, ANSI/AISC 360-16 assumes that the steel can reach its yield stress while the concrete reaches a stress of $0.95f_c^{'}$ for circular CFSTs, and the cross-sectional strength of CFSTs is determined by Eq. (14).

$$N_{AISC} = N_p = A_s f_y + 0.95 A_c f_c^{'} \tag{14}$$

For noncompact sections, ANSI/AISC 360-16 relates the development of concrete strength to cross-sectional slenderness λ (=D/t). The equation to determine the strength is given in Eq. (15).

$$N_{AISC} = N_p - \left(\frac{\lambda - \lambda_p}{\lambda_r - \lambda_p}\right)^2 \left(N_p - N_y\right) \tag{15}$$

in which N_p can be determined from Eq. (14), and N_y is equal to $A_s f_y + 0.7 A_c f_c^{'}$.

Eq. (16) is used to determine the cross-sectional strength for slender sections, in which f_{cr} is critical buckling stress of steel tube considering local buckling. The critical buckling stress f_{cr} of circular sections can be calculated in accordance with ANSI/AISC 360-16.

$$N_{AISC} = A_s f_{cr} + 0.7 A_c f_c^{'} \tag{16}$$

For OctCFSTs, the critical buckling stress f_{cr} might be calculated through Eq. (17) [19],

$$f_{cr} = \left(\frac{1.2}{R} - \frac{0.3}{R^2} \right) f_y \tag{17}$$

where R is the modified plate slenderness parameter as defined in Eq. (18). B is the side width of octagonal sections and v is the Poisson's ratio of steel.

$$R = \frac{B}{t} \sqrt{\frac{12(1-\nu^2) f_y}{4\pi^2 E_s}} \tag{18}$$

4.1.3 GB 50936-2014 [21]

Chinese code GB 50936-2014 adopts a unified theory to calculate the cross-sectional strength of OctCFSTs (N_{GB}). The cross-sectional strength N_{GB} is related to the confining factor ξ (as formulated in Eq. (19)) and $f_{ck}(A_s+A_c)$, where f_{ck} is the characteristic compressive strength of concrete that can be converted from concrete compressive cube strength (obtained from 150×150×150 cubes) per GB 50010-2010 [34]. When calculating f_{ck}, the compressive cylinder strength $f_c^{'}$ was firstly converted to cube strength $f_{cu,150}$ using Eq. (20), which has been extensively used in [35-37]. The cube strength $f_{cu,150}$ was subsequently converted to the characteristic strength f_{ck}, as per GB 50010-2010 [34].

$$\xi = \frac{A_s f_y}{A_c f_{ck}} \tag{19}$$

$$f_c^{'} = f_{cu,150} \left[0.76 + 0.2 \log_{10} \left(\frac{f_{cu,150}}{19.6} \right) \right] \tag{20}$$

The relationship among N_{GB}, ξ and $f_{ck}(A_s+A_c)$ is expressed in Eq. (21). The recommended range of confining factor ξ is from 0.5 to 2.0. For a direct comparison between test results and code predictions, in Eqs. (22) and (23), partial factors for steel and concrete (1.105 and 1.4, respectively) were not considered. Hence, the expressions for coefficients B and C in Eqs. (22) and (23) are slightly different from their original forms in GB 50936-2014.

$$N_{GB} = (1.212 + B\xi + C\xi^2)(A_s + A_c) f_{ck} \tag{21}$$

$$B = 0.140 f_y / 235 + 0.778 \tag{22}$$

$$C = -0.070 f_{ck} / 20 + 0.026 \tag{23}$$

4.2 Assessments

It is obvious from the last section that ANSI/AISC 360-16 and Method 1 in EN 1994-1-1 target at control of cross-section yielding. GB 50936-2014 also aims at control of cross-section yielding, as the design formulas are derived based on the first occurrence of N_u or $N_{0.3\%}$, in which N_u is the ultimate load and $N_{0.3\%}$ is the load corresponding to axial strain of 3000$\mu\varepsilon$ [21]. Further to the discussion in Section 3.2, the failure load N_f was taken as the first occurrence of $N_{1.0\%}$ and N_u, to avoid excessive axial deformation. Therefore, the predictions from Method 1 in EN 1994-1-1 ($N_{EC4,1}$), ANSI/AISC 360-16 (N_{AISC}), and GB 50936-2014 (N_{GB}) were compared with the failure load N_f obtained from the tests. Method 2 in EN 1994-1-1 fully accounts the confinement effect, predictions from which were then compared with the ultimate load N_u instead. When compared with EN 1994-1-1 and ANSI/AISC 360-16, the design methods for circular CFSTs were used and the predictions were calculated by substituting the original diameter by the equivalent circumcircle diameter. The results of the assessments against different design codes are presented in Table 7.

The test results were firstly compared with predictions by Method 1 in Eurocode EN 1994-1-1 ($N_{EC4,1}$). Referring to Table 7, the steel contribution ratio δ of all the specimens falls between 0.2 and 0.9, satisfying the requirement, but in terms of the cross-sectional slenderness, majority of the specimens exceed the limit ($90\times235/f_y$). Method 1 conservatively estimates the cross-sectional strength of all OctCFST columns. Among the 20 test results, no $N_f/N_{EC4,1}$ falls below 1.0, even when the cross-section slenderness greatly exceeds the specified limit as shown in Fig. 13(a). The mean value of $N_f/N_{EC4,1}$ ratio is 1.13 with a corresponding CoV of 0.05. In general, the $N_f/N_{EC4,1}$ ratio decreases with the cross-sectional slenderness, but increases with the confinement ratio θ, as illustrated in Figs. 12(a) and 12(b), respectively. Under the same cross-section slenderness, the $N_f/N_{EC4,1}$ ratio of specimens infilled with C90 concrete are smaller than others, which is primarily due to the reduced confinement ratio. As shown in Fig. 13(b), the $N_f/N_{EC4,1}$ ratio for C90 series specimens decreases dramatically when the confinement ratio θ is less than 0.5. This observation may be due to the brittle nature of high strength concrete. Special attention is therefore suggested to be paid to the use of high strength concrete and a confinement ratio θ not smaller than 0.5 is recommended for high strength concrete.

To reasonably evaluate the design efficiency of the Method 2 ($N_{EC4,2}$) in EN 1994-1-1, the ultimate load N_u was used. As shown in Fig. 14, Method 2 slight overestimates the strength in all cases, yielding a mean $N_u/N_{EC4,2}$ value of 0.94 with a corresponding CoV of 0.03. This is largely due to the overestimation of the enhancement in concrete strength caused by confinement (see Eq. (10)), indicating that directly substituting the diameter by the equivalent circumcircle diameter cannot efficiently predict the cross-sectional strength of OctCFST columns. Zhu and Chan [15] proposed an equivalent inscribed circle method D_{ic} based on the Method 2 in Eurocode EN 1994-1-1 to determine the cross-sectional strength of OctCFSTs. In this method, a reduction factor is

adopted to account for the reduced confinement effectiveness in OctCFSTs, making the design formula for circular CFSTs applicable to OctCFSTs. The proposed design equation is given in Eq. (24),

$$N_{ic} = \eta_{a,Dic} A_s f_y + \left(1 + 0.73\eta_{c,Dic} \frac{tf_y}{D_{ic} f_c'}\right) A_c f_c' \quad (24)$$

where D_{ic} (=H) is the inscribed diameter of the octagonal section, $\eta_{a,Dic}$ and $\eta_{c,Dic}$ are the factors calculated from Eqs. (12) and (13) based on the equivalent inscribed circle. As mentioned earlier, the circumcircle method gives slightly more conservative predictions. The inscribed circle D_{ic} in Eq. (24) was replaced by the circumcircle diameter D in the strength calculation. The design equation based on the circumcircle diameter D is expressed in Eq. (25),

$$N_{cc} = \eta_{a,Dcc} A_s f_y + \left(1 + 0.73\eta_{c,Dcc} \frac{tf_y}{Df_c'}\right) A_c f_c' \quad (25)$$

where $\eta_{a,Dcc}$ and $\eta_{c,Dcc}$ are the factors calculated from Eqs. (12) and (13) using the equivalent circumcircle diameter. Evaluation of the inscribed circle (N_{ic}) and circumcircle (N_{cc}) are tabulated in Table 7. Fig. 15 plots the N_u/N_{ic} and N_u/N_{cc} ratios against the cross-sectional slenderness of OctCFST specimens. As indicated by Table 7 and Fig. 15, both inscribed circle and circumcircle methods produce reasonable strength predictions with the N_u/N_{ic} and N_u/N_{cc} ratios marginal to unity. The mean N_u/N_{ic} and N_u/N_{cc} values are 0.99 and 1.01 with corresponding CoVs of 0.03 and 0.03, respectively. In general, the circumcircle method offers slightly better predictions than the inscribed circle method. It is also noted that the N_u/N_{ic} and N_u/N_{cc} ratios decrease with the increase of cross-section slenderness. By adopting the circumcircle method, the cross-section slenderness can be safely extended to $135\times235/f_y$, in accordance with GB 50936-2014.

Fig. 16 shows the evaluation results of ANSI/AISC 360-16. As shown, ANSI/AISC 360-16 produces safe but conservative cross-sectional strength predictions for OctCFST columns than EN

1994-1-1. This is because the contribution of concrete in ANSI/AISC 360-16 is multiplied by a coefficient of 0.95 for compact sections, which is lower than the specified value (1.0) in EN 1994-1-1. With the cross-section classification considered, the strengths of compact, noncompact and slender sections were computed using Eqs. (14) to (16), respectively. The critical buckling stress f_{cr} of slender octagonal sections was calculated from Eqs. (17) and (18). The mean value of N_f/N_{AISC} is 1.23 and the corresponding CoV is 0.06. When the test results were compared with predictions only using the design equation for compact sections (denoted as $N_{AISC,p}$), the mean value of N_f/N_{AISC} reduces to 1.17 with the corresponding CoV increasing to 0.04. Overall, ANSI/AISC 360-16 underestimates the cross-sectional strength of OctCFSTs.

The applicability of the Chinese code GB 50936-2014 is depicted in Fig. 16. As shown, GB 50936-2014 gives satisfactory strength predictions (N_{GB}) for the OctCFST specimens in this study. Among the twenty specimens, only one N_f/N_{GB} falls below unity. It is noted that the cross-section slenderness of this specimen exceeds the specified limit ($135\times235/f_y$). The mean N_f/N_{GB} ratio of 1.05 and the corresponding CoV is 0.04. As indicated in Fig. 17, the current slenderness limit for circular CFSTs can be safely extended to the design of octagonal CFSTs when the circumcircle method is adopted.

In summary, Method 1 in EN 1994-1-1 and ANSI/AISC 360-16 conservatively predict the cross-sectional strength of OctCFSTs. When the equivalent circumcircle method is directly used, Method 2 in EN 1994-1-1 overpredicts the capacities of OctCFSTs due to the overestimation of the confinement effect. The proposed circumcircle method and GB 50936-2014 produce excellent cross-sectional strength predictions for the OctCFSTs. The slenderness limit specified in GB 50936-2014 for circular CFSTs can be extended to the design of octagonal CFSTs if the circumcircle method and the method in GB 50936-2014 are used.

5. Conclusions

An experimental investigation into effect of concrete infill on the compressive behaviour of compact to slender OctHSs has been presented in this paper. In total, twenty OctCFST stub column specimens were prepared and tested. Five OctHSs with different cross-section slenderness (from compact to slender) were used. The OctHSs were cold-formed from 3 and 6 mm 460 steel plates with measured yield strengths of 546.5 and 580.7 MPa, respectively. Three grades of concrete with target concrete cylinder strength of 30, 50 and 90 MPa were used to infill the hollow tubes. The stub column test results together with measured geometric properties have been reported in detail.

Experimental results demonstrate that for each cross-section with the increase of f_c' the ultimate load N_u improved significantly, but the load dropped more rapidly after N_u was attained due to the brittleness of high strength concrete and reduced confinement effectiveness. Experimental results also indicate that the material strengths of both steel and concrete in the OctCFST short columns can be fully utilised. The strength index (*SI*) of all the specimens is greater than unity and *SI* generally increases with the increase of confinement ratio. The test results were then compared with the strength predictions calculated from EN 1994-1-1, ANSI/AISC 360-16, GB 50936-2014 and the equivalent circle methods. Overall, it has been found that Method 1 in Eurocode EN 1994-1-1 and ANSI/AISC 360-16 safely but conservatively calculate the cross-sectional strength, while Method 2 overpredicts the strength due to overestimation of confinement in OctCFSTs. The circumcircle method and GB 50936-2014 give excellent cross-sectional strength predictions for the OctCFSTs. The current slenderness limit specified for circular CFSTs in GB 50936-2014 can be safely extended to the design of high strength OctCFSTs if the circumcircle method and GB 50936-2014 are used.

Acknowledgement

The research work presented in this paper was supported by a grant from the Research Grants Council of the Hong Kong Special Administrative Region, China (Project no. 152492/16E). The support from the Chinese National Engineering Research Centre for Steel Construction (Hong Kong Branch) at The Hong Kong Polytechnic University is also appreciated.

Reference

[1] J. Chen, H. Fang, T.-M. Chan, Design of fixed-ended octagonal shaped steel hollow sections in compression, Engineering Structures 228 (2021).

[2] H. Fang, T.-M. Chan, B. Young, Behavior of Octagonal High-Strength Steel Tubular Stub Columns, Journal of Structural Engineering 145(12) (2019).

[3] J. Chen, J.-Y. Zhu, T.-M. Chan, Experimental and numerical investigation on stub column behaviour of cold-formed octagonal hollow sections, Engineering Structures 214 (2020).

[4] J. Chen, H. Liu, T.-M. Chan, Material properties and residual stresses of cold-formed octagonal hollow sections, Journal of Constructional Steel Research 170 (2020).

[5] R.M. Slocum, Considerations in the design and fabrication of tubular steel transmission structures. , The fifteenth International Symposium on Tubular Structures - ISTS 15, Rio de Janeiro, Brazil, 2015.

[6] ASCE, Design of steel transmission pole structures, ASCE/SEI 48-11, American Society of Civil Engineers (ASCE), Reston, Virginia, 2011.

[7] CEN, Eurocode 3: Design of steel structures - Part 1.1: General rules and rules for buildings, EN 1993-1-1, European Committee for Standardization (CEN), Brussels,Belgium, 2005.

[8] AISC, Specification for structural steel buildings., ANSI/AISC 360-16, American Institute of Steel Construction (AISC). Chicago, IL, USA., 2016.

[9] H. Fang, T.-M. Chan, B. Young, Material properties and residual stresses of octagonal high strength steel hollow sections, Journal of Constructional Steel Research 148 (2018) 479-490.

[10] J.-Y. Zhu, T.-M. Chan, B. Young, Cross-sectional capacity of octagonal tubular steel stub columns under uniaxial compression, Engineering Structures 184 (2019) 480-494.

[11] Y. Migita, Y. Fukumoto, Local buckling behaviour of polygonal sections, Journal of Constructional Steel Research 41(2/3) (1997) 221-233.

[12] A. Godat, F. Legeron, D. Bazonga, Stability investigation of local buckling behavior of tubular polygon columns under concentric compression, Thin-Walled Structures 53 (2012) 131-140.

[13] K.A.S. Susantha, H. Ge, T. Usami, Uniaxial stress–strain relationship of concrete confined by various shaped steel tubes, Engineering Structures 23 (2001) 1331-1347.

[14] F.-x. Ding, Z. Li, S. Cheng, Z.-w. Yu, Composite action of octagonal concrete-filled steel tubular stub columns under axial loading, Thin-Walled Structures 107 (2016) 453-461.

[15] J.-Y. Zhu, T.-M. Chan, Experimental investigation on octagonal concrete filled steel stub columns under uniaxial compression, Journal of Constructional Steel Research 147 (2018) 457-467.

[16] J.-Y. Zhu, T.-M. Chan, Behaviour of polygonal-shaped steel-tube columns filled with high-strength concrete, Proceedings of the Institution of Civil Engineers - Structures and Buildings 171(2) (2018) 96-112.

[17] J. Chen, T.-M. Chan, Experimental assessment of the flexural behaviour of concrete-filled steel tubular beams with octagonal sections, Engineering Structures 199 (2019).

[18] J. Chen, T.-M. Chan, R.K.L. Su, J.M. Castro, Experimental assessment of the cyclic behaviour of concrete-filled steel tubular beam-columns with octagonal sections, Engineering Structures 180 (2019) 544-560.

[19] J.-J. Lim, T.-S. Eom, Compression tests of octagonal concrete-filled thin-walled tube columns, Engineering Structures 221 (2020).

[20] M. Tomii, K. Yoshimura, Y. Morishita, Experimental studies on concrete-filled steel tubular stub columns under concentric loading, International Colloquium on Stability of Structures Under Static and Dynamic Loads, American Society of Civil Engineers (ASCE), Washington, DC, USA., 1977, pp. 718-741.

[21] CABP, Technical code for concrete-filled steel tubular structures [in Chinese], GB 50936-2014, China Architecture & Building Press (CABP), Beijing, China, 2014.

[22] CEN, Eurocode 4: Design of composite steel and concrete structures Part 1-1: General rules and rules for buildings, EN 1994-1-1, European Committee for Standardization (CEN), Brussels, Belgium, 2009.

[23] R.D. Ziemian, Stability Design Criteria for Metal Structures, Sixth ed., John Wiley & Sons, Inc., Hoboken, New Jersey, 2010.

[24] CEN, Metallic materials - tensile testing. Part 1: Method of test at ambient temperature, EN ISO 6892-1, European Committee for Standardization (CEN), Brussels, Belgium, 2019.

[25] CEN, Testing Hardened Concrete: Compressive Strength of Test Specimens, EN 12390-3, European Committee for Standardization (CEN), Brussels, Belgium, 2009.

[26] L.-H. Han, Concrete Filled Steel Tubular Structures - Theory and Practice [in Chinese], Third ed., Science Press, Beijing, China, 2016.

[27] L.-H. Han, Tests on stub columns of concrete-filled RHS sections, Journal of Constructional Steel Research 58(3) (2002) 353-372.

[28] Z. Tao, Z.-B. Wang, Q. Yu, Finite element modelling of concrete-filled steel stub columns under axial compression, Journal of Constructional Steel Research 89 (2013) 121-131.

[29] Z.-B. Wang, Z. Tao, L.-H. Han, B. Uy, D. Lam, W.-H. Kang, Strength, stiffness and ductility of concrete-filled steel columns under axial compression, Engineering Structures 135 (2017) 209-221.

[30] M. Pandey, B. Young, Tests of cold-formed high strength steel tubular T-joints, Thin-Walled Structures 143 (2019).

[31] ACI, Guide for the Design and Construction of Externally Bonded FRP Systems for Strengthening Concrete Structures, ACI 440.2R-08, merican Concrete Institute (ACI), Farmington Hills, MI, USA, 2008.

[32] F. Wang, B. Young, L. Gardner, Experimental Study of Square and Rectangular CFDST Sections with Stainless Steel Outer Tubes under Axial Compression, Journal of Structural Engineering 145(11) (2019).

[33] J. Chen, Behaviour and design of high strength circular hollow and concrete-filled tubular stub columns under uniaxial compression, Ph.D thesis, Department of Civil and Environmental Engineering, The Hong Kong Polytechnic University, 2020.

[34] CABP, Code for design of concrete structures [In Chinese], GB 50010-2010, China Academy of Building Research (CABR), Beijing, China, 2010.

[35] K.-H. Reineck, D.A. Kuchma, K.S. Kim, S. Marx, Shear Database for Reinforced Concrete Members without Shear Reinforcement, ACI Structural Journal 100(2) (2003).

[36] K.-H. Reineck, E. Bentz, B. Fitik, D.A. Kuchma, O. Bayrak, ACI-DAfStb Databases for Shear Tests on Slender Reinforced Concrete Beams with Stirrups (with Appendix), ACI Structural Journal 111(5) (2014).

[37] J. Chen, T.-M. Chan, K.-F. Chung, Design of square and rectangular CFST cross-sectional capacities in compression, Journal of Constructional Steel Research 176 (2021).

Table 1. Geometric properties of OctCFST specimens.

Specimen	H	B	D	t	L	r_o	r_i	b	A_s	A_c	ρ	$b/(t\varepsilon)$	Classi-fication[1]	H/t	Classi-fication[2]	D/t	Classi-fication[3]
	mm	mm	mm	mm	mm	mm	mm	mm	mm^2	mm^2	%						
O60×3-30	146.8	60.8	158.9	3.05	433	7.0	3.5	55.0	1457	16481	8.1	27.5	Non-slender	48.2	Compact	52.1	Compact
O60×3-50	147.6	61.1	159.7	3.04	431	6.5	3.5	55.7	1450	16664	8.0	28.0	Non-slender	48.5	Compact	52.5	Compact
O60×3-50#	147.4	61.0	159.5	3.06	432	7.0	3.5	55.2	1467	16604	8.1	27.5	Non-slender	48.2	Compact	52.2	Compact
O60×3-90	147.6	61.1	159.7	3.04	432	7.0	3.5	55.3	1461	16663	8.1	27.8	Non-slender	48.5	Compact	52.5	Compact
O75×3-30	184.6	76.5	199.8	3.05	539	7.0	4.0	70.7	1829	26501	6.5	35.3	Slender	60.5	Noncompact	65.5	Noncompact
O75×3-50	184.6	76.4	199.8	3.06	540	7.0	4.0	70.6	1833	26478	6.5	35.2	Slender	60.3	Noncompact	65.3	Noncompact
O75×3-90	184.5	76.4	199.7	3.04	543	7.0	3.5	70.6	1834	26444	6.5	35.4	Slender	60.6	Noncompact	65.6	Noncompact
O75×3-90#	182.8	75.7	197.8	3.02	543	7.0	3.5	69.9	1804	25954	6.5	35.3	Slender	60.5	Noncompact	65.5	Noncompact
O75×6-30	187.0	77.5	202.4	5.85	544	11.0	5.0	68.3	3501	25615	12.0	18.4	Non-slender	32.0	Compact	34.6	Compact
O75×6-50	187.1	77.5	202.5	5.86	544	11.0	5.0	68.4	3508	25631	12.0	18.3	Non-slender	31.9	Compact	34.5	Compact
O75×6-90	186.8	77.4	202.2	5.79	543	11.0	5.0	68.3	3463	25594	11.9	18.5	Non-slender	32.3	Compact	34.9	Compact
O75×6-90#	186.4	77.2	201.7	5.82	543	11.0	5.0	68.1	3472	25458	12.0	18.4	Non-slender	32.0	Compact	34.7	Compact
O90×3-30	220.9	91.5	239.1	3.04	646	7.5	4.0	85.3	2199	38325	5.4	42.8	Slender	72.7	Noncompact	78.7	Slender
O90×3-50	220.6	91.4	238.8	3.05	647	7.0	3.5	85.6	2202	38208	5.4	42.8	Slender	72.4	Noncompact	78.4	Slender
O90×3-90	219.7	91.0	237.8	3.05	648	7.0	3.5	85.2	2193	37890	5.5	42.6	Slender	72.1	Noncompact	78.0	Slender
O90×3-90#	220.7	91.4	238.9	3.05	649	7.0	3.5	85.6	2204	38229	5.5	42.8	Slender	72.4	Noncompact	78.3	Slender
O105×3-30	257.1	106.5	278.3	3.03	755	7.0	4.0	100.7	2542	52312	4.6	50.7	Slender	84.9	Slender	91.9	Slender
O105×3-30#	256.8	106.4	278.0	3.04	753	7.0	4.0	100.6	2550	52198	4.7	50.5	Slender	84.5	Slender	91.5	Slender
O105×3-50	256.6	106.3	277.8	3.04	756	7.0	3.5	100.5	2558	52084	4.7	50.5	Slender	84.5	Slender	91.4	Slender
O105×3-90	256.6	106.3	277.7	3.03	759	7.0	3.5	100.5	2553	52063	4.7	50.5	Slender	84.6	Slender	91.6	Slender

Note: # indicates a repeated test;

ε is the material coefficient depending on f_y ($\varepsilon = \sqrt{235/f_y}$);

[1] cross-section classifications based on the criterion for OctHSs proposed in [1];

[2] cross-section classifications according to ANSI/AISC 360-16 when equivalent inscribed circle method is used;

[3] cross-section classifications according to ANSI/AISC 360-16 when equivalent circumcircle method is used.

Table 2. Measured material properties of steel.

Steel	E_s	v	f_y	f_u	ε_{sh}	ε_u	ε_f
	GPa		MPa	MPa	%	%	%
3 mm	209.5 (0.005)	0.28	546.5 (0.003)	625.8 (0.006)	2.2	10.9	26.0
6 mm	213.3 (0.005)	0.28	580.7 (0.002)	666.1 (0.004)	2.3	10.1	25.4

Note: Values in the brackets are the corresponding coefficients of variation (CoV).

Table 3. Measured material properties of concrete.

Grades	E_c	v	f_c'	ε_c
	GPa		MPa	%
C30-1	25.3 (0.01)	0.18	27.9 (0.01)	0.202
C30-2	29.8 (0.04)	0.19	32.3 (0.03)	0.210
C50	52.7 (0.03)	0.19	55.0 (0.02)	0.246
C90	42.9 (0.03)	0.19	92.1 (0.05)	0.277

Note: Values in the brackets are the corresponding coefficients of variation (CoV).

Table 4. Test results of OctCFST stub columns.

Specimen	f_y MPa	f_c' MPa	θ	N_0 kN	N_u kN	ε_u %	SI	$N_{1.0\%}$ kN	N_f kN	DI	$(EA)_{sc}$ $\times 10^3$kN	$(EA)_{sc,Cal}$ $\times 10^3$kN	$\varepsilon_{y,sc}$ %	$\varepsilon_u/\varepsilon_{y,sc}$	Cross-section Classification[c]
O60×3-30	546.5	32.3	1.50	1328	1616	1.53	1.22	1605	1605	-[b]	752	796	0.18	8.66	Compact
O60×3-50	546.5	55.0	0.86	1709	2053	0.65	1.20	1989	2053	2.51	1007	849	0.17	3.83	Compact
O60×3-50#	546.5	55.0	0.88	1715	1982	0.66	1.16	1891	1982	2.35	935	850	0.18	3.60	Compact
O60×3-90	546.5	92.1	0.52	2333	2565	0.50	1.10	2308	2565	2.42	1005	1021	0.23	2.15	Compact
O75×3-30	546.5	27.9	1.35	1739	2046	1.45	1.18	2033	2033	-[b]	1003	1054	0.17	8.36	Noncompact
O75×3-50	546.5	55.0	0.69	2458	2903	0.49	1.18	2574	2903	2.39	1169	1250	0.21	2.33	Noncompact
O75×3-90	546.5	92.1	0.41	3438	3702	0.40	1.08	-[a]	3702	1.53	1391	1519	0.25	1.62	Noncompact
O75×3-90#	546.5	92.1	0.41	3376	3753	0.41	1.11	-[a]	3753	1.41	1378	1491	0.25	1.67	Noncompact
O75×6-30	580.7	27.9	2.85	2748	3550	4.51	1.29	3194	3194	-[b]	1343	1395	0.20	22.04	Compact
O75×6-50	580.7	55.0	1.45	3447	4211	0.95	1.22	4197	4211	-[b]	1628	1586	0.21	4.49	Compact
O75×6-90	580.7	92.1	0.85	4368	5098	0.65	1.17	4935	5098	2.37	1816	1837	0.24	2.70	Compact
O75×6-90#	580.7	92.1	0.86	4361	5033	0.63	1.15	4743	5033	2.44	1844	1833	0.24	2.66	Compact
O90×3-30	546.5	27.9	1.12	2271	2532	0.69	1.12	2517	2532	-[b]	1274	1430	0.18	3.87	Slender
O90×3-50	546.5	55.0	0.57	3305	3695	0.46	1.12	2866	3695	1.76	1751	1711	0.19	2.44	Slender
O90×3-90	546.5	92.1	0.34	4688	4891	0.44	1.04	3102	4891	1.34	1993	2085	0.24	1.87	Slender
O90×3-90#	546.5	92.1	0.34	4726	5116	0.44	1.08	3211	5116	1.50	1893	2102	0.25	1.76	Slender
O105×3-30	546.5	32.3	0.82	3079	3527	0.67	1.15	3453	3527	-[b]	1812	2092	0.17	3.94	Slender
O105×3-30#	546.5	32.3	0.83	3080	3538	0.44	1.15	3441	3538	4.45	1972	2090	0.16	2.82	Slender
O105×3-50	546.5	55.0	0.49	4262	4641	0.41	1.09	3581	4641	1.83	2384	2239	0.18	2.29	Slender
O105×3-90	546.5	92.1	0.29	6190	6317	0.37	1.02	4804	6317	1.49	2946	2768	0.21	1.76	Slender

Note: # indicates a repeated test.

a: Tests were terminated before 1.0% axial strain was reached.

b: The axial load does not drop back to 85% of the ultimate load.

c: The section classification was based on the circumcircle method using the criteria for circular CFSTs.

Table 5. Summary of the selected circular CFST specimens in [33].

Specimen	D	t	L	D/t	f_y	f_c'	A_s	A_c	θ	N_0	N_u	ε_u	SI	Cross-section Classification according to ANSI/AISC 360-16
	mm	mm	mm		MPa	MPa	mm^2	mm^2		kN	kN	%		
4C200×3-30	200.7	3.02	597	66.4	571.7	33.5	1877	29764	1.08	2070	2605	2.31	1.26	Noncompact
4C200×3-50	201.9	3.05	599	66.2	571.7	51.9	1905	30101	0.70	2651	3204	0.85	1.21	Noncompact
4C200×3-90	200.7	3.07	598	65.4	571.7	94.9	1905	29727	0.39	3910	4197	0.56	1.07	Noncompact
4C200×6-30	199.6	5.84	599	34.2	630.3	33.5	3555	27720	2.41	3169	4154	3.81	1.31	Compact
4C200×6-50	199.4	5.82	600	34.3	630.3	51.9	3539	27678	1.55	3667	4587	2.00	1.25	Compact
4C200×6-90	199.9	5.87	601	34.1	630.3	94.9	3579	27819	0.85	4896	5747	1.15	1.17	Compact

Table 6. Range of applicability of current design codes for circular CFST columns.

Codes	f_y MPa	f_c' MPa	λ_p	λ_r	λ_{max}	Other requirements
EN 1994-1-1 [22]	235-460	20-50	$90\times235/f_y$	-	$90\times235/f_y$	$0.2 \le \delta \le 0.9$
ANSI/AISC 360-16 [8]	≤525	21-69	$0.15E_s/f_y$ ($128\times235/f_y$)	$0.19E_s/f_y$ ($162\times235/f_y$)	$0.31\times E_s/f_y$ ($264\times235/f_y$)	$\rho \ge 1\%$
GB 50936-2014 [21]	235-460	30-80[a]	$135\times235/f_y$	-	$135\times235/f_y$	-

Note: a: concrete compressive cube strength.

Values in the brackets are equivalent slenderness limits assuming E_s = 200 GPa.

Table 7. Assessment of different design methods for OctCFSTs.

Specimen	$D/[t(235/f_y)]$	δ	$N_{EC4,1}$	$N_f/N_{EC4,1}$	$N_{EC4,2}$	$N_u/N_{EC4,2}$	N_{ic}	N_u/N_{ic}	N_{cc}	N_u/N_{cc}	N_{AISC}	N_f/N_{AISC}	$N_{AISC,p}$	$N_f/N_{AISC,p}$	N_{GB}	N_f/N_{GB}
			kN		kN		kN		kN		kN		kN		kN	
O60×3-30	121.3	0.578	1328	1.21	1739	0.93	1619	1.00	1585	1.02	1302	1.23	1302	1.23	1497	1.07
O60×3-50	122.2	0.464	1709	1.20	2101	0.98	1986	1.03	1953	1.05	1663	1.23	1663	1.23	1848	1.11
O60×3-50#	121.3	0.467	1715	1.16	2106	0.94	1991	1.00	1957	1.01	1669	1.19	1669	1.19	1854	1.07
O60×3-90	122.2	0.342	2333	1.10	2699	0.95	2590	0.99	2558	1.00	2256	1.14	2256	1.14	2426	1.06
O75×3-30	152.2	0.575	1739	1.17	2273	0.90	2118	0.97	2074	0.99	1699	1.20	1702	1.19	1979	1.03
O75×3-50	151.8	0.408	2458	1.18	2956	0.98	2810	1.03	2769	1.05	2380	1.22	2385	1.22	2654	1.09
O75×3-90	152.6	0.292	3438	1.08	3896	0.95	3759	0.98	3720	1.00	3306	1.12	3316	1.12	3549	1.04
O75×3-90#	152.3	0.292	3376	1.11	3824	0.98	3690	1.02	3652	1.03	3248	1.16	3257	1.15	3486	1.08
O75×6-30	85.5	0.740	2748	1.16	3766	0.94	3465	1.02	3379	1.05	2712	1.18	2712	1.18	3063	1.04
O75×6-50	85.3	0.591	3447	1.22	4421	0.95	4132	1.02	4049	1.04	3376	1.25	3376	1.25	3699	1.14
O75×6-90	86.3	0.460	4368	1.17	5282	0.97	5008	1.02	4929	1.03	4250	1.20	4250	1.20	4565	1.12
O75×6-90#	85.7	0.462	4361	1.15	5275	0.95	5001	1.01	4922	1.02	4244	1.19	4244	1.19	4556	1.10
O90×3-30	183.0	0.529	2271	1.12	2910	0.87	2725	0.93	2672	0.95	2112	1.20	2217	1.14	2590	0.98
O90×3-50	182.2	0.364	3305	1.12	3898	0.95	3724	0.99	3674	1.01	3002	1.23	3200	1.15	3557	1.04
O90×3-90	181.5	0.256	4688	1.04	5234	0.93	5072	0.96	5025	0.97	4197	1.17	4514	1.08	4808	1.02
O90×3-90#	182.1	0.255	4726	1.08	5275	0.97	5112	1.00	5065	1.01	4219	1.21	4550	1.12	4846	1.06
O105×3-30	213.8	0.429	3079	1.15	3826	0.92	3610	0.98	3548	0.99	2572	1.37	2995	1.18	3497	1.01
O105×3-30#	212.7	0.431	3080	1.15	3829	0.92	3612	0.98	3550	1.00	2574	1.37	2995	1.18	3497	1.01
O105×3-50	212.7	0.328	4262	1.09	4949	0.94	4748	0.98	4690	0.99	3403	1.36	4119	1.13	4573	1.01
O105×3-90	213.0	0.225	6190	1.02	6822	0.93	6635	0.95	6581	0.96	4752	1.33	5950	1.06	6309	1.00
Mean				1.13		0.94		0.99		1.01		1.23		1.17		1.05
CoV				0.05		0.03		0.03		0.03		0.06		0.04		0.04

Note: # indicates a repeated test.

Fig. 1. Use of octagonal hollow section (West Lafayette, US).

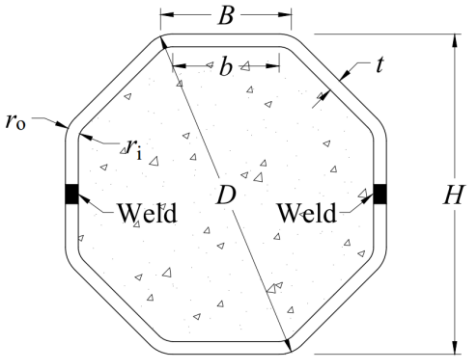

(a) OctCFST section

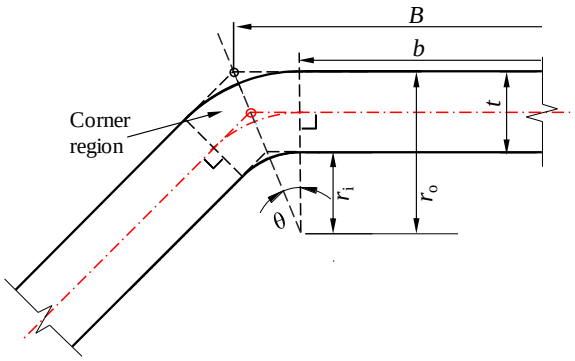

(b) Corner portion of OctHS

Fig. 2. Definition of symbols.

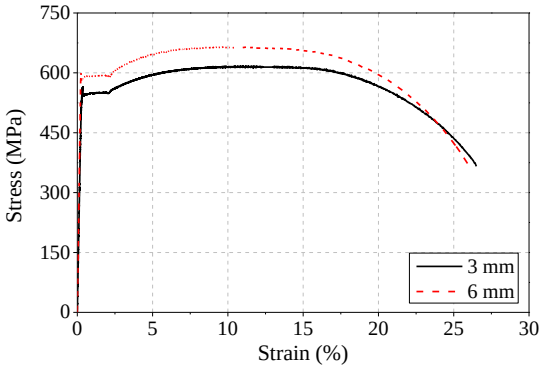

Fig. 3. Typical stress-strain curves of steel.

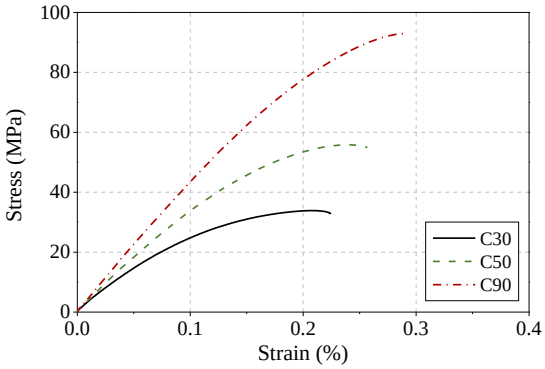

Fig. 4. Typical stress-strain curves of concrete.

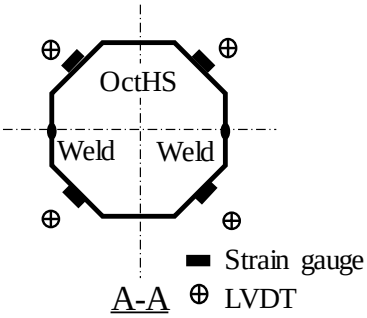

(a) Instrumentations of strain gauges and LVDTs

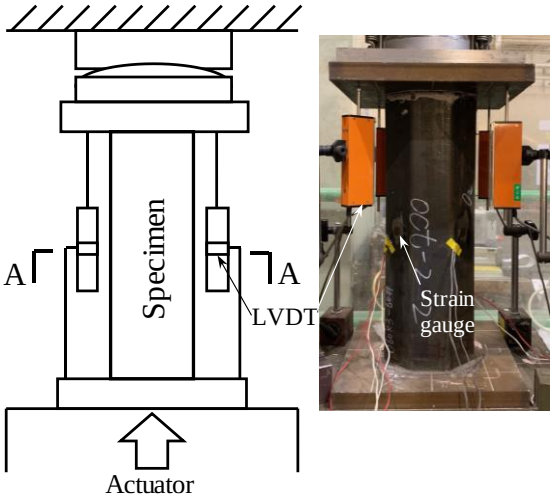

(b) MTS 4600kN hydraulic testing machine

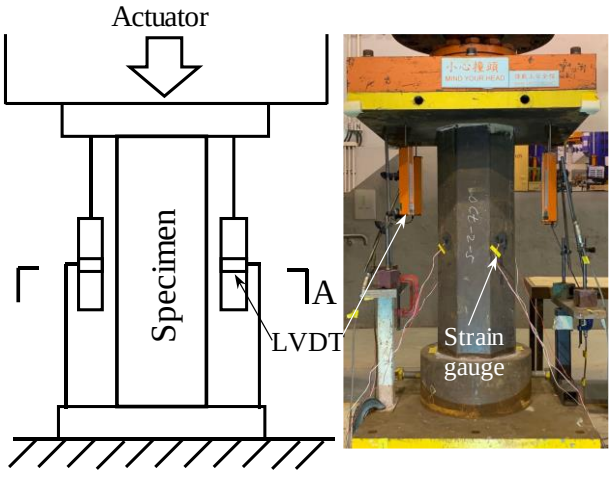

(c) 10000 kN universal servo-controlled testing machine

Fig. 5. OctCFST stub column test arrangements.

Fig. 6. Typical failure modes (Specimen O75×3-90).

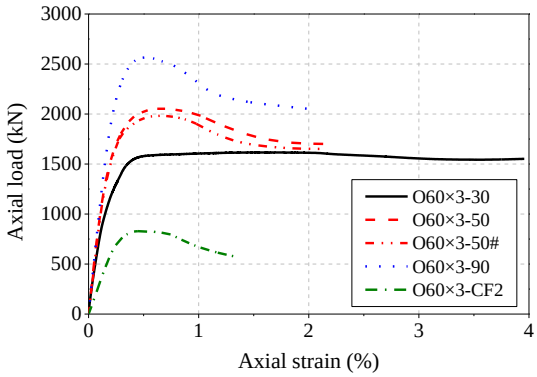

(a) O60×3

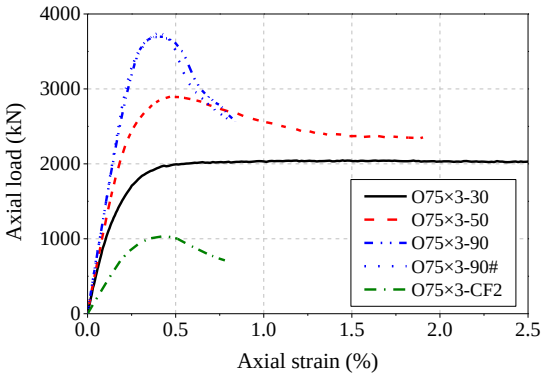

(b) O75×3

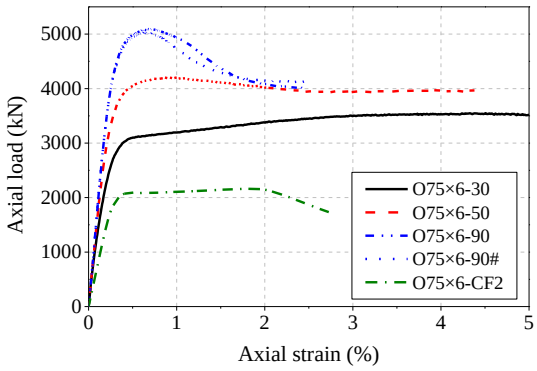

(c) O75×6

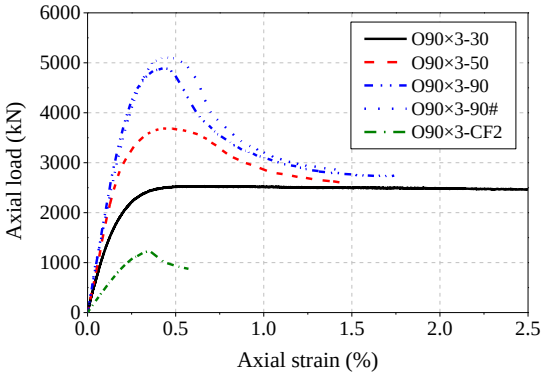

(d) O90×3

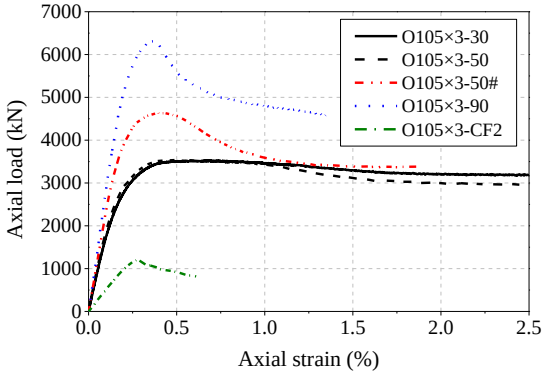

(e) O105×3

Fig. 7. Axial load versus axial strain curves for OCFST stub columns (# indicates a repeated test).

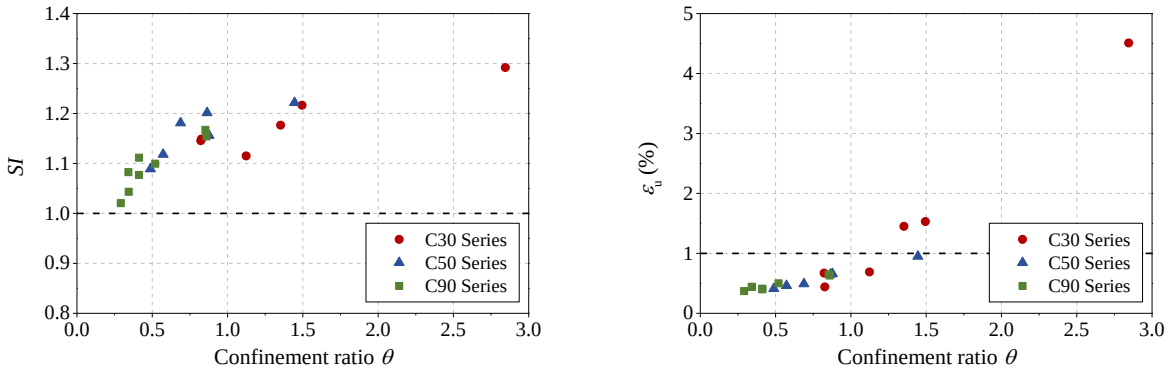

(a) Strength index *SI* (b) Ultimate axial strain ε_u

Fig. 8. Influence of confinement ratio θ.

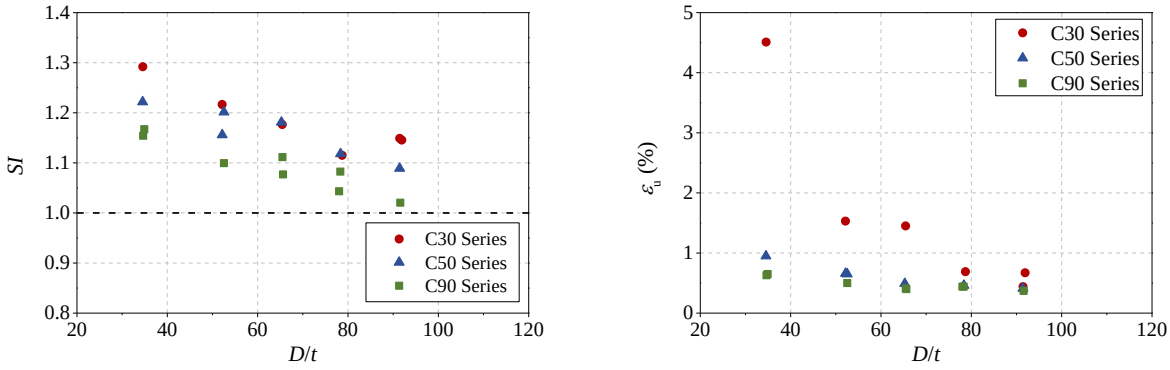

(a) Strength index *SI* (b) Ultimate axial strain ε_u

Fig. 9. Influence of cross section slenderness.

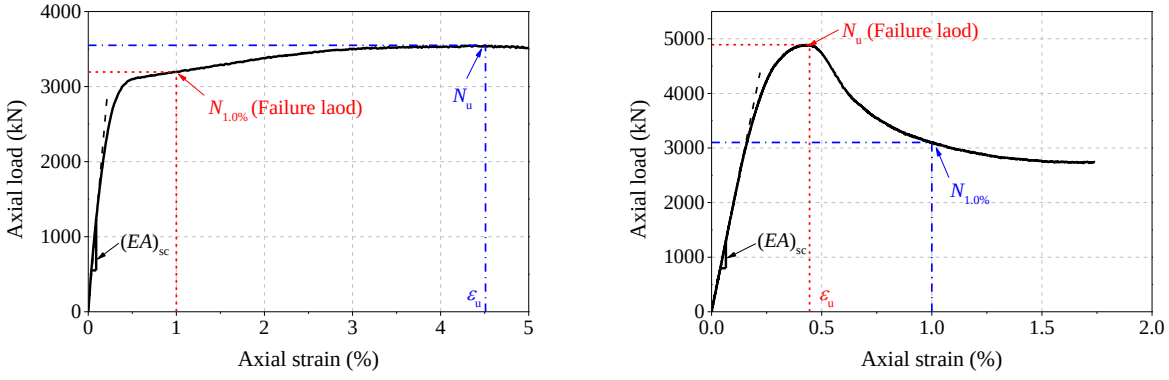

(a) $\varepsilon_u \geq 1.0\%$ (b) $\varepsilon_u < 1.0\%$

Fig. 10. Definition of failure load N_f.

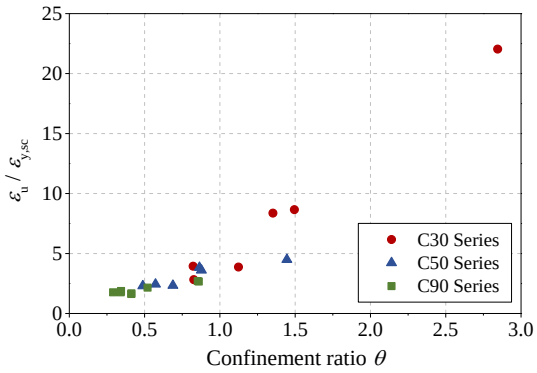

Fig. 11. Effect of confinement ratio θ on $\varepsilon_u/\varepsilon_{y,sc}$.

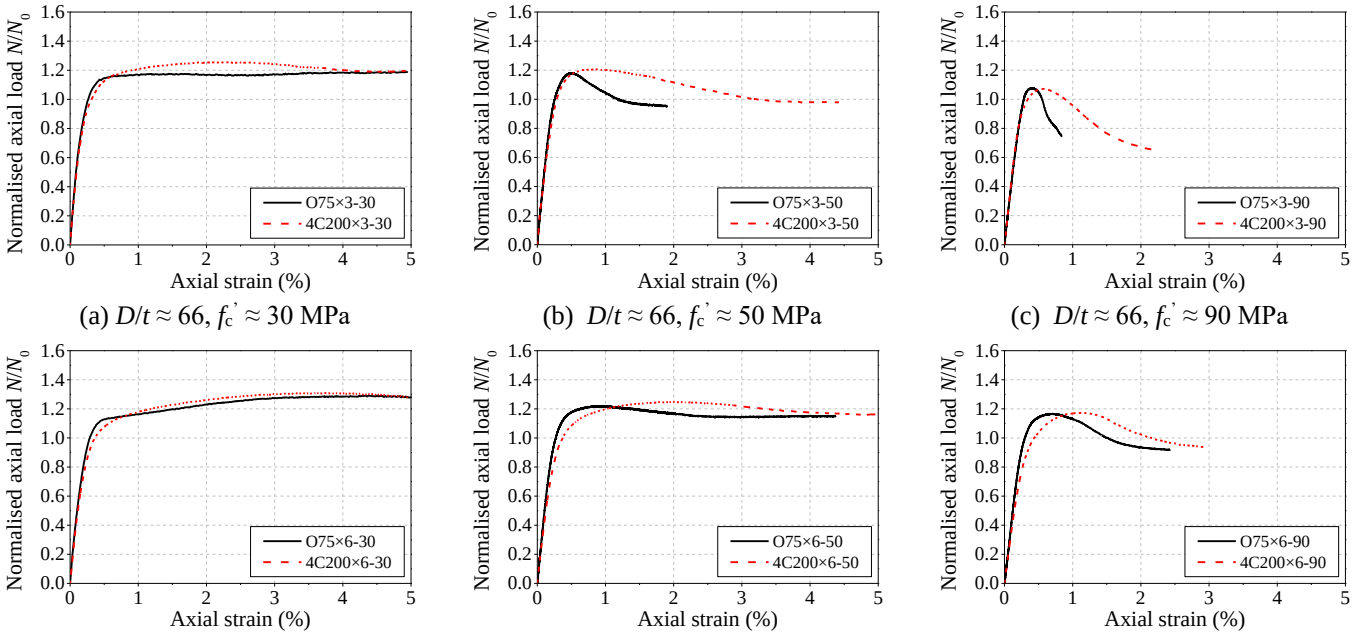

(a) $D/t \approx 66$, $f_c' \approx 30$ MPa (b) $D/t \approx 66$, $f_c' \approx 50$ MPa (c) $D/t \approx 66$, $f_c' \approx 90$ MPa

(d) $D/t \approx 34$, $f_c' \approx 30$ MPa (e) $D/t \approx 34$, $f_c' \approx 50$ MPa (f) $D/t \approx 34$, $f_c' \approx 30$ MPa

Fig. 12. Comparison of selected circular CFSTs from [33] with OctCFSTs.

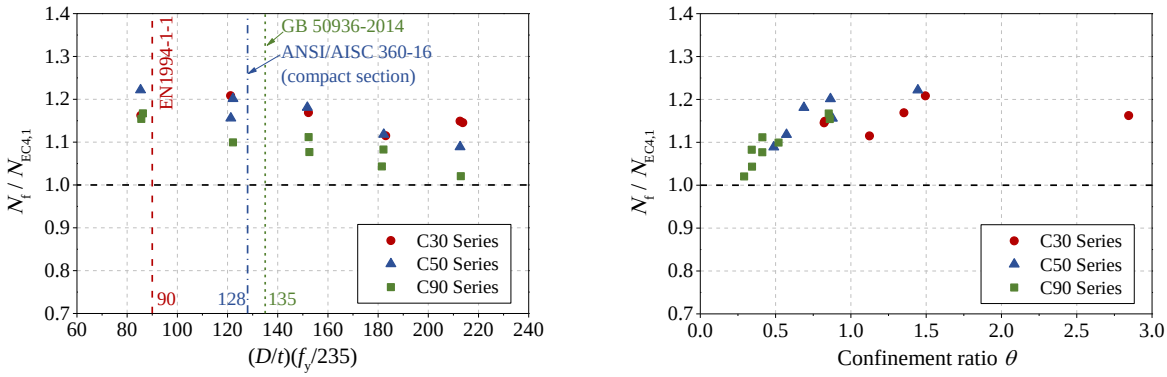

(a) Versus cross-section slenderness (b) Versus confinement ratio θ

Fig. 13. Comparison of experimental cross-sectional strengths with predicted strengths using Method 1 in EN 1994-1-1.

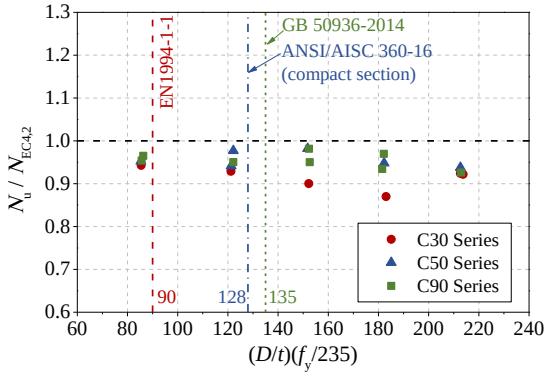

Fig. 14. Comparison of experimental cross-sectional strengths with predicted strengths using Method 2 (equivalent circumcircle method) in EN 1994-1-1.

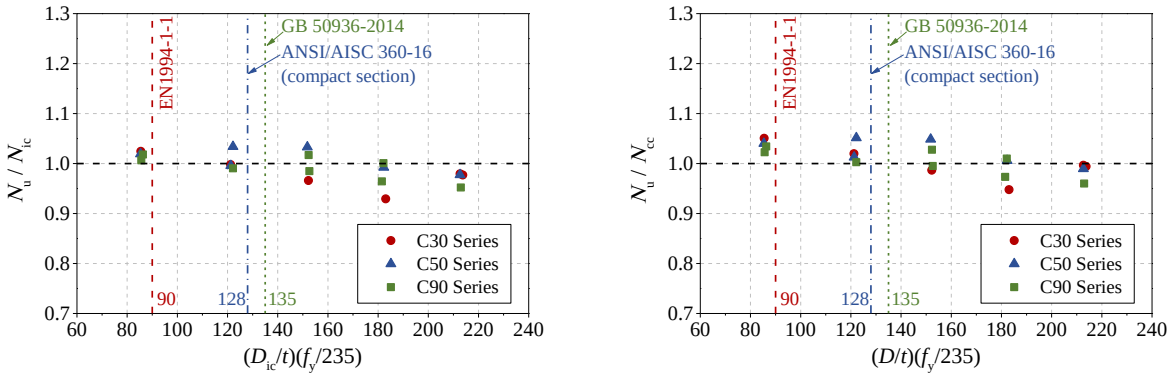

(a) Inscribed circle method (b) Circumcircle method

Fig. 15. Comparison of experimental cross-sectional strengths with predicted strengths using equivalent circle methods.

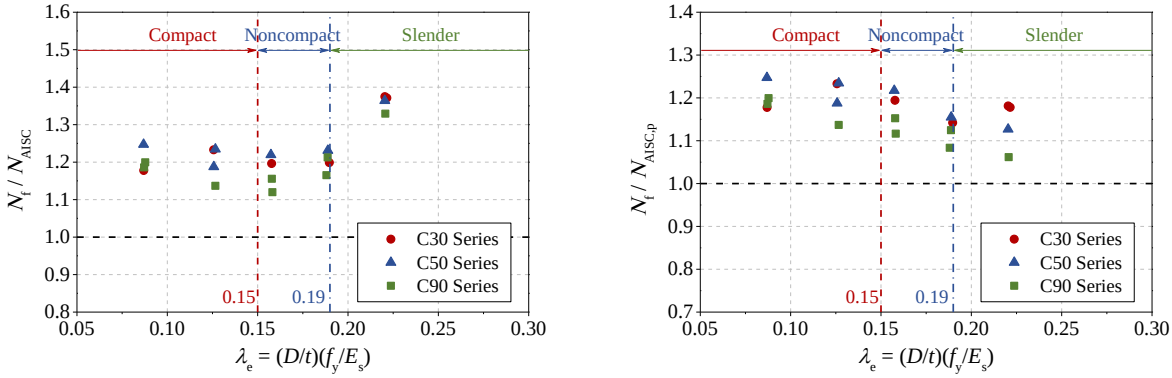

(a) N_{AISC} (b) $N_{AISC,p}$

Fig. 16. Comparison of experimental cross-sectional strengths with predicted strengths using ANSI/AISC 360-16.

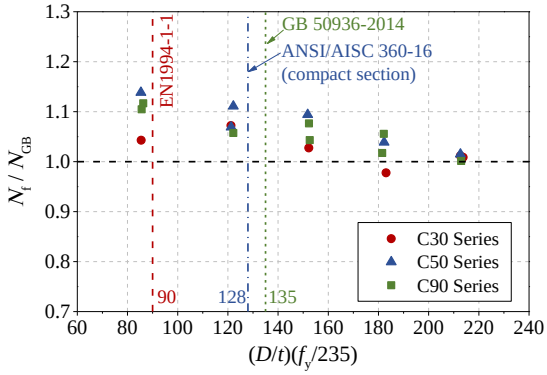

Fig. 17. Comparison of experimental cross-sectional strengths with predicted strengths using GB 50936-2014.